OPTICAL TWEEZERS FOR SINGLE MOLECULE BIOLOGY

ANDERS WALLIN

Department of Physics
Faculty of Science
University of Helsinki
February 2011

ACADEMIC DISSERTATION

To be presented with the permission of the Faculty of Science of the University of Helsinki for public criticism in auditorium XII of the Univeristy of Helsinki main building, Unioninkatu 34, on May 24th, 2011, at 12 o'clock noon.

SUPERVISORS

Professor Edward Hæggström
Department of Physics
University of Helsinki
Finland

Dr. Roman Tuma
Astbury Centre for Structural Molecular Biology
University of Leeds
United Kingdom

REVIEWERS

Professor Nynke Dekker
Kavli Institute of Nanoscience
TU Delft
The Netherlands

Dr. David Brockwell
Astbury Centre for Structural Molecular Biology
University of Leeds
United Kingdom

OPPONENT

Professor Antoine van Oijen
Zernike Institute for Advanced Materials
University of Groningen
The Netherlands

Report Series in Physics HU-P-D181
ISBN 978-952-10-6879-9 (printed version)
ISBN 978-952-10-6880-5 (PDF http://ethesis.helsinki.fi/)
ISSN 0356-0961

ABSTRACT

Molecular machinery on the micro-scale, believed to be the fundamental building blocks of life, involve forces of 1-100 pN and movements of nanometers to micrometers. Micromechanical single-molecule experiments seek to understand the physics of nucleic acids, molecular motors, and other biological systems through direct measurement of forces and displacements. Optical tweezers are a popular choice among several complementary techniques for sensitive force-spectroscopy in the field of single molecule biology. The main objective of this thesis was to design and construct an optical tweezers instrument capable of investigating the physics of molecular motors and mechanisms of protein/nucleic-acid interactions on the single-molecule level.

A double-trap optical tweezers instrument incorporating acousto-optic trap-steering, two independent detection channels, and a real-time digital controller was built. A numerical simulation and a theoretical study was performed to assess the signal-to-noise ratio in a constant-force molecular motor stepping experiment. Real-time feedback control of optical tweezers was explored in three studies. Position-clamping was implemented and compared to theoretical models using both proportional and predictive control. A force-clamp was implemented and tested with a DNA-tether in presence of the enzyme lambda exonuclease.

The results of the study indicate that the presented models describing signal-to-noise ratio in constant-force experiments and feedback control experiments in optical tweezers agree well with experimental data. The effective trap stiffness can be increased by an order of magnitude using the presented position-clamping method. The force-clamp can be used for constant-force experiments, and the results from a proof-of-principle experiment, in which the enzyme lambda exonuclease converts double-stranded DNA to single-stranded DNA, agree with previous research.

The results on estimating the signal-to-noise ratio in constant-force assays can guide the design of future experiments. The results on feedback control on the micro scale have broader implications for other techniques dominated by Brownian motion such as magnetic tweezers or scanning probe microscopy. The proof-of-principle single molecule experiment with lambda exonuclease shows that the developed instrument can be used to investigate a variety of molecular motors and protein/nucleic-acid interactions. The main objective of the thesis was thus achieved. The developed instrument and presented results on feedback control serve as a stepping stone for future contributions to the growing field of single molecule biology.

Anders Wallin, Optical tweezers for single molecule biology, February 2011, 37 pages. University of Helsinki, Report Series in Physics HU-P-D181
Classification (PACS): 87.80.Cc Optical trapping, 87.80.Nj Single-molecule techniques, 07.60.-j Optical instruments and equipment, 07.05.Dz Control systems.

PUBLICATIONS

This thesis consists of a summary and the following original publications, which are referred to in the text by Roman numerals (**I** – **IV**).

I. **A.E. Wallin**, A. Salmi, and R. Tuma, *Step Length Measurement – Theory and Simulation for Tethered Bead Constant Force Single Molecule Assay*, Biophysical Journal **93** 795-805 (2007)
doi:10.1529/biophysj.106.097915

II. **A.E. Wallin**, H. Ojala, E. Hæggström, and R. Tuma, *Stiffer optical tweezers through real-time feedback control*, Applied Physics Letters **92** 224104 (2008)
doi:10.1063/1.2940339

III. H. Ojala, A. Korsbäck, **A.E. Wallin**, and E. Hæggström, *Optical position clamping with predictive control*, Applied Physics Letters **95** 181104 (2009)
doi:10.1063/1.3257693

IV. **A.E. Wallin**, H. Ojala, G. Ziedaite, and E. Hæggström, *Dual-trap optical tweezers with real-time force clamp control*, submitted for publication.

Papers **I-IV** are reprinted with permission from the publishers.

AUTHOR'S CONTRIBUTION

In **I** the author developed the computational model, derived the theory, performed the simulations, and wrote the paper. In **II** the author designed, constructed, and calibrated the optical tweezers instrument, performed the experiments, and wrote the paper. In **III** the author supervised the development by A.K. and H.O. of the feedback-algorithm, assisted with experiments on the instrument built by the author, and co-authored the paper. In **IV** the author assisted with experiments on the instrument built by the author, co-developed the theory with H.O., and wrote the paper.

ACKNOWLEDGMENTS

The study was conducted at the Electronics Laboratory, Department of Physics, at the University of Helsinki, Finland. I thank the head of the department, prof. Juhani Keinonen, for providing a stimulating environment for the research.

I thank my supervisors prof. Edward Hæggström and Dr. Roman Tuma for their advice and guidance during the project. Prof. Dennis Bamford has provided guidance and insight from a biological point of view. Dr. Jiri Lisal introduced me to both molecular motors and optical trapping in the beginning of the project. During the course of the project I have supervised the B.Sc. theses of Mr. Ville Heikkinen, Mr. Anders Korsbäck, and Mr. Antti Rahikkala as well as the M.Sc. theses of Mr. Heikki Ojala, Mr. Antti Rahikkala, and Mr. Kalle Hanhijärvi. All have contributed towards this thesis, and I have probably learned at least as much as they have during the process. Mr. Ari Salmi developed an early version of the Brownian dynamics simulation during a summer internship. Dr. Gabija Ziedaite has been an essential help on the molecular biology side of things.

I thank my reviewers, prof. Nynke Dekker and Dr. David Brockwell, and my opponent prof. Antoine van Oijen, for accepting and undertaking the task of reviewing this thesis.

I am grateful for financial support from the National Graduate School of Nanosciences and the Jenny and Antti Wihuri foundation. I have been able to attend international conferences through travel grants awarded by the Magnus Ehrnrooth foundation, the Chancellor of the University of Helsinki, and National Instruments Finland.

Anders Wallin, February 2011

CONTENTS

Abbreviations

AAF Anti-Alias Filter

ADC Analog to Digital Converter

AFM Atomic Force Microscope

AMP Amplifier

AOD Acousto Optic Deflector

BSA Bovine Serum Albumin

COND Microscope Condensor

CW Continous Wave

DAC Digital to Analog Converter

DDS Digital Direct Synthesizer

DNA Deoxyribonucleic Acid

EDTA Ethylenediaminetetraacetic Acid

FI Faraday Isolator

FPGA Field Programmable Gate Array

HWP Half-Wave Plate

MM Molecular Motor

OBJ Microscope Objective

PBS Polarizing Beam-Splitter

PD Position Sensitive Detector

PEEK Polyether Ether Ketone

PI Proportional Integral control

PSD Power Spectral Density

PWD Pair-wise distance distribution

RF Radio Frequency

RMS Root Mean Square

SMF Single Mode Fiber

SNR Signal to Noise Ratio

TEW Tris EDTA Tween buffer

WLC Worm-like Chain

Symbols

α Predictive control parameter

d Bead diameter

$\triangle$ Sampling time

ΔL Step length of molecular motor

f Frequency

F_c Clamp force

F_{err} Force clamp error

f_{LP} Measurement bandwidth

F_{set} Force clamp set-point

F_T Random force due to thermal noise

F_{WLC} Restoring force of WLC

γ Hydrodynamic drag coefficient

k_B Boltzmann constant

k_{cat} Enzymatic rate

k_{DNA} Local stiffness of DNA tether

k_{eff} Effective trap stiffness

K_I Integral feedback gain

K_P Proportional feedback gain

L Contour length

λ Wavelength of light

L_p Persistence length

n Refractive index

ω Angular frequency

T Temperature

τ	Feedback loop delay
$\triangle t$	Simulation time step
x_e	Equilibrium extension
x_{set}	Position clamp set-point

1 INTRODUCTION

1.1 FORCE-SPECTROSCOPY IN SINGLE MOLECULE BIOLOGY

Forces on the molecular scale range from 10 nN required e.g. to break a covalent bond down to <1 pN required e.g. to stretch a DNA-molecule significantly[1]. Micromechanical force spectroscopy experiments[2] that seek to measure forces on the molecular scale commonly use atomic force microscopes (AFMs), optical tweezers[3, 4, 5], or magnetic tweezers. While the AFM can be used to break covalent bonds or unfold proteins at high forces[6], and while the magnetic tweezers technique excels at low force (<1 pN) and torque experiments[7, 8], optical tweezers are a popular choice for single-molecule experiments in biology[9, 10, 11] due to its intermediate force range (ca. 1-100 pN) and high spatial resolution (<1 nm).

Single molecule biology[12, 13] studies the smallest constituents of life with novel tools[14, 15] that permit manipulation, imaging, and interrogation of single macromolecules. Observing single molecules avoids ensemble averaging and allows seeing new molecular mechanisms, rare and transient events, and reveals both static and dynamic heterogeneity in these mechanisms[16, 17].

1.2 OPTICAL TWEEZERS

Gradient optical tweezers use focused laser light to trap, manipulate, and measure forces on dielectric particles. The force on a trapped particle is due to a change in the momentum of the light. The total optical force is usually divided into a gradient force acting in the direction of the intensity gradient of the light, and a scattering force acting in the direction of the incident light[18]. Trapping is stable when the gradient force which pulls particles towards the beam focus exceeds the scattering force which pushes particles away from the focus in the direction of the incident light. When trapping particles of size d with light of wavelength λ, force calculations can be performed in the ray-optics regime ($d \gg \lambda$)[19], the intermediate Mie-regime ($d \approx \lambda$)[20], or the Rayleigh-regime ($d \ll \lambda$)[5]. A Gaussian beam profile is usually employed when trapping particles with a higher refractive index than the surrounding medium, e.g. polystyrene or silica ($n \sim 1.5$) beads in water ($n = 1.33$).

Optical tweezers instruments are commonly built either around inverted research microscopes[21], or as custom instruments in the laboratory[22]. The trapping laser wavelength is usually in the near-infrared, to minimize optical damage to specimens[23], and either a single laser beam[21], or dual counter propagating beams[24] are employed. High resolution

measurement of trapped bead position is performed by back-focal-plane interferometry[25] using a position sensitive photodetector that detects either forward- or back-scattered[26] light from the trapping laser or from a separate low power detection beam. Experiments with nucleic acid tethers are typically performed by tethering the molecule between an optically trapped bead and the cover slip surface[27], or another bead[28]. The other bead can be held in a micropipette, or in a 'dumbbell' experiment, held by another optical trap. The dumbbell geometry decouples the experiment from the microscope stage and thus avoids drift and noise from e.g. thermal expansion of the microscope[29]. In most experiments either a force-extension curve is measured, or changes in the tether length are observed. Thus a need to steer one or both of the optical traps exists. Steering can be performed by introducing steering mirrors, a spatial light modulator[30], or an acousto-optic deflector (AOD) in the trapping beam path. For high resolution experiments[31] or high speed time-sharing experiments[32] the AOD has proven most popular.

Because the thermal energy at physiological- or room-temperature is of the same order (~4 pNnm) as other forces/displacements experienced by a typical biomolecule, thermal noise is an essential part of experiments at the micro- or nano-scale. Experimentally measured signals contain a thermal noise component that limits the achievable signal-to-noise ratio[33]. Zero-mean random noise can be avoided by low-pass filtering and increasing the duration of the experiment, up to a point where instrumental drift or other pink (1/f) noise sources dominate.

1.3 FEEDBACK CONTROL OF OPTICAL TWEEZERS

Feedback control[34] has been used in optical tweezers instruments since their inception[4, 35]. Position clamp (isometric) control aims to stabilize the trapped particle position, i.e. increase the effective trap stiffness. Force clamp (isotonic) control strives to maintain a constant tension in e.g. a tethered biomolecule, corresponding to a zero trap stiffness, independent of tether length changes.

Feedback control can be performed by moving the microscope stage [36, 22], by adjusting the trap laser intensity[4, 37], or by steering the trap with 1D[38] or 2D[21] acousto-optic deflectors, steering mirrors[39], or a spatial light modulator[40]. Combining AODs and a deformable mirror for steering along the optical axis allows 3D control of trap position[41, 42]. An alternative approach for constant force experiments is to create a constant optical gradient[43] or to use the constant force region of the trapping potential[44, 45].

Force clamp experiments are often preferred since the analysis and interpretation of constant force data is straightforward. Observing a compliant tether at constant force eliminates a signal due to the elasticity of the tether[33]. Constant force experiments have been performed to observe e.g. molecular motors[28] and DNA/RNA hairpin unfolding[46].

1.4 AIMS AND SCOPE OF THE RESEARCH

The aim of this thesis was to design and construct an optical tweezers instrument capable of investigating the physics of molecular motors and mechanisms of protein/nucleic-acid interactions on the single-molecule level.

Paper **I** asks how the experimental parameters in a typical constant force molecular motor experiment affect the signal-to-noise ratio (SNR). What SNR is required to extract the step length of a molecular motor? How can this SNR be achieved? For a model experiment a theoretical expression as well as approximate equations for the SNR are derived. Numerical simulations of the model are performed and the SNR extracted from simulations is compared to the theoretical prediction. Both theory and simulations are compared to previously published single molecule experiments.

Paper **II** asks if the effective trap stiffness can be increased by position clamp real-time feedback control. What is the maximum effective trap stiffness that can be achieved? What limits maximum effective trap stiffness? An optical tweezers instrument with an AOD-steerable trapping beam and two independent detection lasers and detectors is presented. A data acquisition card incorporating a field-programmable gate array (FPGA) is used to implement a proportional control position clamp feedback algorithm in real-time. One detection laser is used in-loop for feedback control, while the other detection laser provides independent out-of-loop data on which later analysis is based. The power spectral density (PSD) of bead position time series and the effective trap stiffness is compared to theoretical predictions. The results from **II** indicated that the loop delay and the associated resonance peak in the bead position PSD limits the maximum achievable effective trap stiffness.

Paper **III** asks whether higher effective trap stiffness can be achieved with another control algorithm? A new position clamp control algorithm, termed predictive control, is introduced. An increased effective trap stiffness is achieved using predictive control instead of proportional control. The PSD of bead position fluctuations is compared to a theoretical prediction.

Paper **IV** asks if constant force single molecule experiments can be performed using the real-time controller presented in **II** and **III**? How much can force noise be reduced? Can the force clamp be modeled, and does experiment agree with theory? A dual-trap optical tweezers instrument with real-time active constant force feedback control is presented. Two proof-of-principle force clamp experiments are performed. In the first experiment a DNA molecule was held force clamped and the bead position and tether tension PSDs were compared to theoretical predictions. In the second experiment a DNA molecule was force clamped in the presence of bacteriophage lambda exonuclease and the enzymatic shortening of the tether was observed.

2

METHODS

2.1 MODELING OPTICAL TWEEZERS EXPERIMENTS

2.1.1 *Predicting SNR in constant-force experiments*

Paper **I** considers a simplified model for a constant force single molecule experiment (Figure 1) where a bead of diameter d is held in a force clamp with tension F_c. The bead is tethered to a stationary wall through a tether modeled as a worm-like chain (WLC) of length L with persistence length L_p. The effect of a molecular motor (MM) translocating along the tether is modeled by shortening the contour length in discrete steps of length ΔL at an average rate k_{cat}. In experiments the bead position $x(t)$ is measured. In thermal equilibrium the WLC produces a restoring force

$$F_{WLC}(x,\, L) = \frac{k_B T}{L_p}\left(\frac{1}{4}\left(1-\frac{x}{L}\right)^{-2} - \frac{1}{4} + \frac{x}{L}\right). \tag{2.1}$$

The force-clamp extends the tether until $F_{WLC}(x_e,\, L) = F_C$, where x_e is the equilibrium extension. Around this equilibrium position, ignoring the inertia of the bead, the linearized equation of motion for the bead is

$$\gamma \dot{x} = k_{DNA}(x_e - x) + F_T, \tag{2.2}$$

where γ is the hydrodynamic drag coefficient of the bead, F_T is the thermal random force on the bead with power spectral density $4\gamma k_B T$, and k_{DNA} is the local stiffness of the WLC

$$k_{DNA} = \left.\frac{dF_{WLC}}{dx}\right|_{x=x_e}. \tag{2.3}$$

When the contour length changes to $L - \triangle L$, the bead moves to a new equilibrium where $F_{WLC}(x_e + \triangle x_e,\, L - \triangle L) = F_C$. To first order the extension change (signal) is (see **I**)

$$\triangle x_e = -\frac{x_e}{L}\triangle L. \tag{2.4}$$

The amplitude signal-to-noise ratio (SNR) can now be defined as

$$SNR = \frac{\triangle x_e}{x_{RMS}}, \tag{2.5}$$

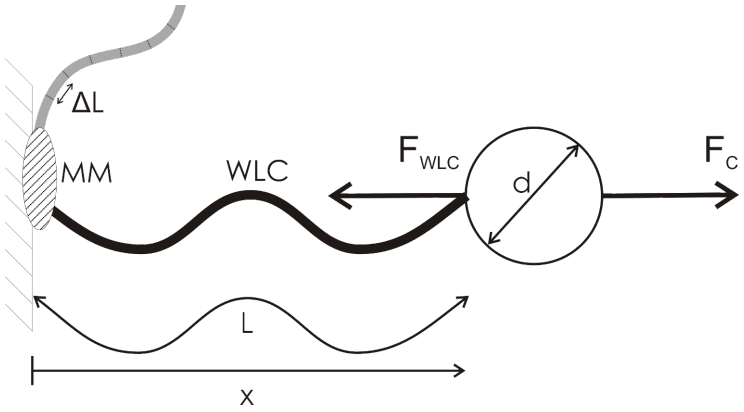

Figure 1: Model for constant force single molecule experiment. A bead of diameter d is tethered to a molecular motor MM through a worm-like chain (WLC) of contour length L and extension x. An external clamp-force F_C is balanced by the WLC restoring force F_{WLC}. The step length of the molecular motor is $\triangle L$.

where x_{RMS} is the root-mean-square (RMS) of the position fluctuation of the bead due to thermal motion. In a given measurement bandwidth f_{LP} the RMS thermal force is $F_{T,RMS} = \sqrt{4\gamma k_B T f_{LP}}$, and thus x_{RMS} is

$$x_{RMS} = \frac{F_{T,RMS}}{k_{DNA}} = \frac{\sqrt{4\gamma k_B T f_{LP}}}{k_{DNA}}. \tag{2.6}$$

Inserting Eq. (2.6) into Eq. (2.5) gives an expression for the SNR as a function of the model parameters:

$$SNR = \frac{x_e}{L} \frac{\triangle L}{\sqrt{4\gamma k_B T f_{LP}}} k_{DNA}. \tag{2.7}$$

Using Eq. (2.7) requires solving Eq. (2.1) for x_e and then calculating k_{DNA} with Eq. (2.3). Paper **I** therefore presents approximate equations for the SNR where x_e and k_{DNA} have been eliminated. Table 2 in paper **I** lists SNR values from recently published single molecule experiments.

2.1.2 *Brownian motion simulation and analysis*

Numerical simulations of the model experiment in Figure 1 were performed to verify the analytically predicted SNR (Eq. (2.7)). The equation of motion, ignoring inertia, for the bead

$$\gamma \dot{x} = F_C - F_{WLC} + F_T, \tag{2.8}$$

was numerically solved using the Euler-method[47] with a time step $\triangle t$. The bead-position x_j at time-step j was calculated as

$$x_j = x_{j-1} + \frac{\triangle t}{\gamma}(F_C - F_{WLC} + F_T), \tag{2.9}$$

and the random force F_T in a bandwidth from 0 Hz to the Nyquist frequency $f_{LP} = \frac{1}{2\triangle t}$ was

$$F_T = N(0,1)\sqrt{4k_BT\gamma f_{LP}}, \tag{2.10}$$

where $N(0,1)$ is a normally distributed random number with zero mean and unit variance. Normally distributed pseudo random numbers were generated with the Mersenne twister[48] and Box-Muller[49] algorithms. During the simulation the WLC contour length was shortened by ΔL at an average rate k_{cat}. A time step of $\triangle t = 0.1\,\mu$s was used in all simulations. This time step was found by decreasing $\triangle t$ until the PSD of the bead position did not change significantly. The simulation was implemented as a MEX-file in C and called from MATLAB. Pseudo code for the simulation is presented in Appendix A.

The SNR of a simulated time series of bead position was extracted by first low-pass filtering the time series, then calculating the pair-wise distance distribution (PWD), and its Fourier transform $\widetilde{PWD}$. Steps in the time series generate a peak near $\omega_{\Delta L} = \frac{2\pi}{\triangle L}$, whose normalized height $\widetilde{PWD}(\omega_{\triangle L})/\widetilde{PWD}(0)$ is related to the SNR by (see **I**)

$$SNR = \sqrt{-\frac{(2\pi)^2}{\ln\left(\widetilde{PWD}(\omega_{\triangle L})/\widetilde{PWD}(0)\right)}}. \tag{2.11}$$

2.1.3 *Position-clamp control of optical tweezers*

Papers **II** and **III** model position clamp control of optical tweezers and compare these models to experimental data. A plot of the measured PSD of the bead position fluctuations is commonly used for calibrating optical tweezers. For a harmonic trap the bead position PSD is a Lorentzian[50]. Expressions for the PSDs of bead/trap position and force fluctuation during real-time position clamping and force clamping are derived here.

The equation of motion for the position x of a bead with negligible inertia held in a trap with stiffness k positioned at x_T is

(Figure 2, top)

$$\gamma\dot{x} + k\,(x - x_T) = F_T. \tag{2.12}$$

A proportional position clamp aims to minimize x_{RMS} by steering x_{trap} according to

$$x_T(t) = K_P\left(x_{set} - x\left(t-\tau\right)\right), \tag{2.13}$$

where K_P is the proportional gain, x_{set} is the position set-point, and τ accounts for the delay between the position measurement and the trap steering. Substituting Eq. (2.13) into Eq. (2.12) yields the power spectral density for bead position fluctuations in a proportional position clamp

$$|\widetilde{x}|^2 = \frac{4k_BT\gamma}{|i\omega\gamma + kK_P\exp\left(-i\omega\tau\right) + k|^2}. \tag{2.14}$$

Note that Eq. (2.14) reduces to a Lorentzian when $K_P = 0$. The delay τ between position measurement and trap steering causes a resonance peak at $\omega \approx {}^{2\pi}/_{4\tau}$ to appear in the PSD when K_P is increased. A comparison between the predicted and measured PSD during proportional position clamping is shown in Figure 9.

An alternative to proportional control, termed predictive control, is introduced in **III**, by noting that Eq. (2.13) does not account for bead motion during the acquisition/steering time τ. The predictive controller replaces $x(t-\tau)$ in Eq. (2.13) by a predicted bead position x_p (see Appendix C)

$$\begin{gathered} x_p(t) = x(t-3\triangle) \\ -\alpha\left[3x(t-3\triangle) - x_T(t-\triangle) - x_T(t-2\triangle) - x_T(t-3\triangle)\right]. \end{gathered} \tag{2.15}$$

where $\alpha = 1-\exp\left(-k\triangle/\gamma\right)$, the sampling time of the digital controller is $\triangle$, and $\tau = 3\triangle$ is assumed ($\tau \approx 15\,\mu$s and $\Delta = 5\,\mu$s for our hardware). The PSD for bead position using the predictive controller, Eq. (2.15), is

$$|\tilde{x}|^2 = 4k_BT\gamma\left|i\omega\gamma + \frac{kK_Pe^{-i\omega\tau}\left(1-3\alpha\right)}{1+K_P\alpha\left[e^{-i\omega\triangle}+e^{-i\omega2\triangle}+e^{-i\omega3\triangle}\right]} + k\right|^{-2}. \tag{2.16}$$

Note that 2.16 reduces to the result for proportional control, Eq. (2.14), when $\alpha = 0$, and to a Lorentzian when both $K_P = 0$ and $\alpha = 0$. A comparison between the predicted and measured PSD during predictive position clamping is shown in Figure 10.

When a bead is position-clamped using either proportional or predictive control the effective trap stiffness can be defined as

$$k_{eff} = \frac{k_BT}{\langle x^2\rangle} = \frac{k_BT}{\int|\tilde{x}^2|\,d\omega}. \tag{2.17}$$

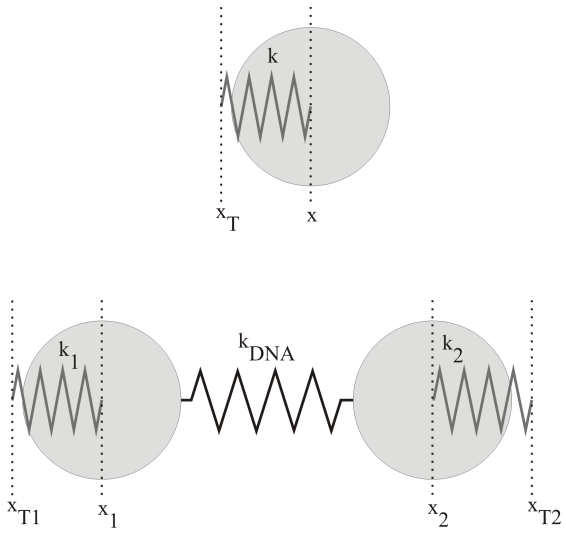

Figure 2: (top) Model for a single optically trapped bead at position x, with trap positioned at x_T, and trap stiffness k. (bottom) Model for dumbbell experiment where a tether of stiffness k_{DNA} is held between two beads at positions x_1 and x_2 by optical traps positioned at x_{T1} and x_{T2} with stiffness k_1 and k_2.

2.1.4 *Force-clamp control of optical tweezers*

A dual-trap optical tweezers instrument with real-time active constant force feedback control is presented in **IV** and in Section 2.2. The predicted PSD for bead position, trap position, and tether tension during force clamping is derived here. A typical 'dumbbell' construct (Figure 2, bottom) consists of two optically levitated beads connected by an elastic DNA tether. Ignoring the inertia of the beads and assuming that over small changes in extension the tether behaves as a Hookean spring, the equation of motion for the system is[51],

$$-\mu^{-1}\dot{\mathbf{x}} - \kappa\mathbf{x} + k\mathbf{x_T} = \mathbf{F_T} \tag{2.18}$$

where $\mathbf{x} = \begin{bmatrix} x_1 & x_2 \end{bmatrix}^T$, $\mathbf{x_T} = \begin{bmatrix} x_{T1} & x_{T2} \end{bmatrix}^T$, and $\mathbf{F_T} = \begin{bmatrix} F_1 & F_2 \end{bmatrix}^T$ denote deviations from an equilibrium position/force. The mobility matrix μ and stiffness matrices κ and k are

$$\mu^{-1} = \begin{pmatrix} \gamma_1 & 0 \\ 0 & \gamma_2 \end{pmatrix}, \kappa = \begin{pmatrix} k_1 + k_{DNA} & -k_{DNA} \\ -k_{DNA} & k_2 + k_{DNA} \end{pmatrix}, k = \begin{pmatrix} k_1 & 0 \\ 0 & k_2 \end{pmatrix}, \tag{2.19}$$

where $\gamma_{1,2}$ is the hydrodynamic drag-coefficient, $k_{1,2}$ denotes trap stiffness, and k_{DNA} is the local spring-constant of the tether. In Eq. (2.19) the hydrodynamic coupling[52] between the beads is omitted, since it is negli-

gible in our experiments using an extended DNA tether that is long (16 µm contour length) compared to the bead radius. In a force clamp experiment the left trap is held stationary ($x_{T1} = 0$) while the right trap is steered using a proportional-integral (PI) controller. The error signal for the PI-controller is given by the difference in measured force in the stationary trap, $k_1 x_1$, compared to a set-point force F_{set}, the desired tether tension. Ignoring constant terms, the position of the steerable trap is

$$x_{T2} = k_1^{-1} \left[K_P F_{err}(t-\tau) + K_I \sum_{n=0}^{\infty} F_{err}(t-\tau-n\triangle) \right], \tag{2.20}$$

where $F_{err} = F_{set} - k_1 x_1$ is the force error and K_P and K_I denote the proportional and integral feedback gains, respectively. Equation 2.20 takes into account the loop delay time τ, i.e. the time it takes for the controller to measure and react by steering the trap, as well as the sampling period $\triangle$, i.e. the data collection interval. Fourier transforming Eq. (2.20) gives

$$\tilde{x}_{T2} = \exp(-i\omega\tau) \left[K_P + K_I \left(1 - \exp(-i\omega\triangle)\right)^{-1} \right] \tilde{x}_1, \tag{2.21}$$

which can be inserted into Eq. (2.18) to yield the equations of motions

$$\begin{aligned} T_1 \tilde{x}_1 + k_{DNA} \tilde{x}_2 &= \tilde{F}_1 \\ T_2 \tilde{x}_2 + \left(k_{DNA} - k_F\right) \tilde{x}_1 &= \tilde{F}_2 \end{aligned} \tag{2.22}$$

where the symbols

$$\begin{aligned} T_j &= -i\omega\gamma_j - k_j - k_{DNA} \\ k_F &= k_2 \exp(-i\omega\tau) \left[K_P + K_I \left(1 - \exp(-i\omega\triangle)\right)^{-1} \right] \end{aligned}, \tag{2.23}$$

have been used. Solving for the Fourier transform of the bead fluctuations gives

$$\tilde{x}_1 = \frac{T_2 \tilde{F}_1 - k_{DNA} \tilde{F}_2}{T_1 T_2 - k_{DNA}^2 + k_{DNA} k_F} \quad \tilde{x}_2 = \frac{T_1 \tilde{F}_2 - \left(k_{DNA} - k_F\right) \tilde{F}_1}{T_1 T_2 - k_{DNA}^2 + k_{DNA} k_F} \tag{2.24}$$

These expressions can be used to find the PSDs of the bead positions $|\tilde{x}_1|^2$ and $|\tilde{x}_2|^2$, as well as the PSDs for the force in the stationary trap, the steerable trap position, and the tether extension fluctuation.

2.2 CONSTRUCTION OF DOUBLE TRAP OPTICAL TWEEZERS

The double trap optical tweezers instrument is built on a pneumatically levitated optical table. A schematic overview of the instrument is shown in Figure 3, and the components of the instrument are listed in Appendix B. The beam from a linearly polarized 4 W 1064 nm CW-laser (1064) is

first collimated (L1:L2), then passed through a Faraday isolator (FI1), and split (PBS1) into a stationary trap beam and steerable trap beam with orthogonal polarizations. The steerable trap beam passes through acousto-optic deflectors (AOD X/Y) while the stationary trap beam can be adjusted manually with gimball-mirrors (M). The trapping beams are combined with another polarizing beam-splitter (PBS2) and steered with telescopes (L3:L4) and (L5:L6) via a dichroic mirror (D2) into an inverted microscope (Nikon TE-2000) so that the plane between the AODs (dashed line) is imaged onto the back-focal-plane of the microscope objective (OBJ).

Position detection of trapped particles is performed with dual detection beams at 785 nm and 830 nm. The light from a temperature stabilized diode-laser (785 and 830) is passed through a Faraday isolator (FI2 and FI3) and coupled to a polarization-maintaining single-mode fiber (SMF) in order to purify the spatial laser mode and to stabilize pointing. Half-wave plates before (HWP2/4) the isolator adjust the intensity of the detection beams. Half-wave plates (HWP3/5) after the isolator align the polarization to the polarization-maintaining axis of the single mode-fiber. The position of the detection lasers in the sample plane is adjustable using gimball-mirrors in the back-focal-plane. The orthogonally polarized detection beams are combined at PBS3, expanded with L7:L8 and combined with the trapping beams at dichroic D1. A high numerical aperture condenser (COND) collects detection light which is deflected towards duolateral position-sensitive detectors (PD1/2) using dichroic D3. A cold-mirror F1 rejects visible light, while a polarizing beam-splitter (PBS4) and laser-line filters centered at 785 nm and 830 nm (F2 and F3) prevent cross talk between the detection channels. A Galilean telescope (L9:L10) collimates the transmitted light, while focusing lenses (L11 and L12) image the condenser back-focal-plane onto the detector surface. In position clamp experiments the two detection lasers can be focused on the same trapped particle and one detection channel is used 'in-loop' for feedback control while the other detection channel collects 'out-of-loop' data independent of the feedback loop. In experiments where the dumbbell extension changes less than ~500 nm one detection laser monitors the bead in the stationary trap while the other detection laser is positioned so that it monitors the steerable bead. In experiments where the extension change is large, the steerable bead can be monitored in a ~500 nm window, outside of which the steerable bead position must be inferred from the position of the steerable trap, the steerable trap stiffness, and the tether tension.

A LED provides bright-field illumination for a CCD-camera. Short pass filters F4 and F5 attenuate the trapping and detection light to prevent saturation of the camera. A tube-lens (TL) internal to the microscope allows switching between 100x and 150x magnification. The sample is positioned on two stacked stages: a piezo-motor stage (PZT1) with 25x25 mm^2 lateral travel and 100 nm resolution provides coarse sample positioning, while a piezoelectric stage (PZT2) with 100x100x30 μm^3 travel provides nanometer resolution positioning. The instrument is controlled by a personal computer running LabVIEW software.

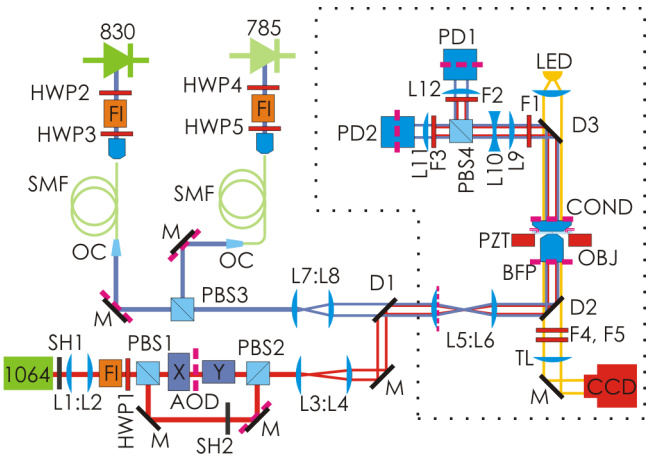

Figure 3: Optical tweezers instrument. Trap laser (1064), diode-lasers for detection (830 and 785), shutter (SH), lens (L), half-wave plate (HWP), Faraday isolator (FI), polarizing beam-splitter (PBS), mirror (M), acousto-optic deflector (AOD), single-mode fiber (SMF), output-coupler (OC), dichroic mirror (D), filter (F), back-focal-plane (BFP), objective (OBJ), piezo-electric stage (PZT), condenser lens (COND), camera (CCD), position-sensitive detector (PD). Components are listed in Table 1.

Figure 4 shows a schematic overview of the control electronics. Data collection, real-time control, and trap steering is performed with a data acquisition card incorporating a Field Programmable Gate Array (FPGA). The FPGA-card allows control algorithms to run in real-time with up to 200 kHz update rate, independently of the host operating system and other computer peripherals. Variable-gain instrumentation amplifiers (AMP) amplify the X and Y detection signals from the PDs so that the response matches the ±10 V input range of the analog to digital converter (ADC). Each PD also provides a sum-signal that is not amplified. Analog voltages are low-pass filtered with a 60 kHz fourth-order Sallen-Key Butterworth anti-aliasing filter (AAF) and then digitized at 200 kS/s with 16-bit precision. Based on the measured detector-voltages a feedback algorithm implemented on the FPGA calculates AOD steering-commands every 5 µs. Two 30-bit digital control words are output to two direct digital synthesizers (DDS) which drive the AODs with an RF-signal at a variable frequency between 25 and 45 MHz and an adjustable amplitude set by a digital to analog (DAC) output on the FPGA card. Manual control of trap position can be performed with two hand-wheels that output quadrature pulses to the FPGA. This allows the operator to position the trap before an experiment begins, or to perform e.g. a force-extension experiment manually. Independent of the feedback-loop both bead and trap position data are logged to disk at a maximal rate of 200 kS/s for later analysis. To reduce disk usage in long duration experiments data can be first collected at 200 kS/s, then digitally low-pass filtered using a digital 2nd order Butterworth low-pass filter on

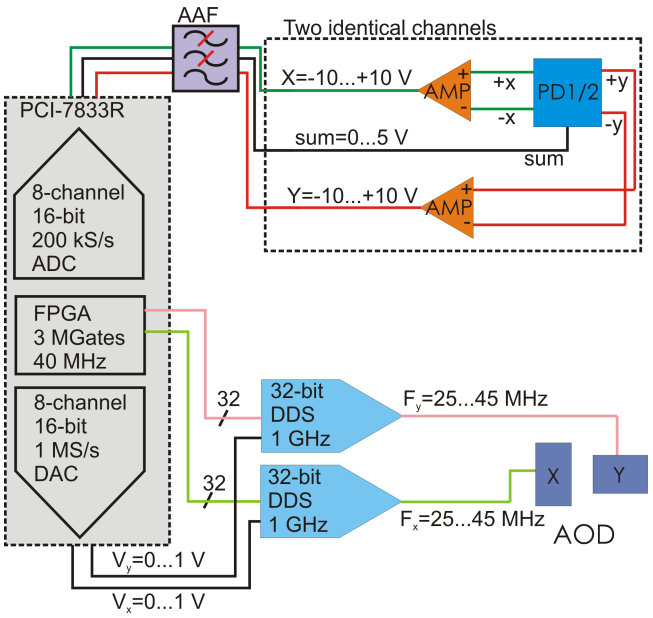

Figure 4: Control electronics of real-time force clamp instrument. Field programmable gate-array (FPGA), analog to digital converter (ADC), digital to analog converter (DAC), anti-alias filter (AAF), position-sensitive detector (PD), differential amplifier (AMP), digital direct synthesizer (DDS), acousto-optic deflector (AOD). Components are listed in Table 2.

the FPGA, and finally saved to disk at a reduced sampling rate. See [53] for schematics of the PD amplifier circuit and the DDS power supply.

2.3 POSITION- AND FORCE-CLAMP EXPERIMENTS

2.3.1 *Sample chamber*

Sample chambers (Figure 5) were assembled by drilling 1.6 mm holes in a 75x25x1 mm^3 microscope slide and by gluing 0.25 mm inner diameter 1/16" PEEK tubing to the slide using UV-curing epoxy (Norland NOA81). A 1-lane or 3-lane pattern was then cut into a 200 µm thick double-stick tape spacer (Tesa) which was glued to the slide. The chamber was sealed with a 60x24x0.17 mm^3 coverslip (Corning). The position-clamp experiments were performed by introducing a bead-solution to the chamber with a syringe pump. The force clamp experiments were performed by trapping beads in lane 1, finding a DNA-tether in lane 2, and performing force-extension and force clamp experiments in lane 3. A syringe pump with 1 ml syringes was used to introduce beads, DNA, and buffer to the chamber at a rate of 1 µl/min.

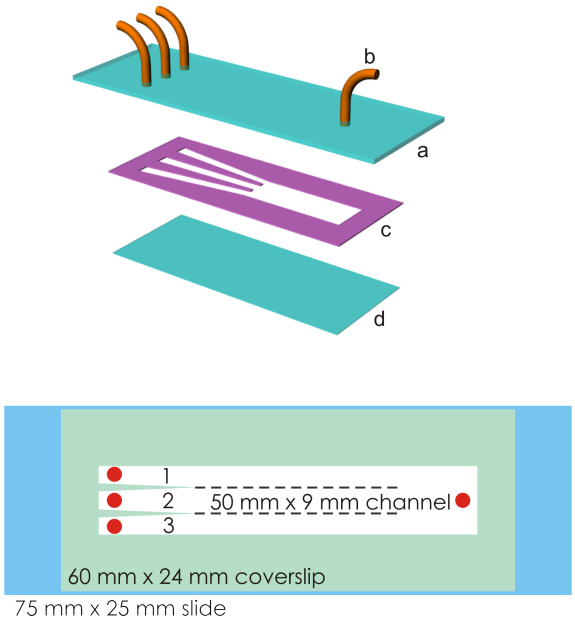

Figure 5: Sample chamber. (a) microscope slide, (b) 1.59 mm (1/16″) outer diameter, 0.25 mm inner diameter PEEK tubing, (c) 200 μm thick double-stick tape spacer, (d) #1.5 170 μm thick coverslip.

2.3.2 *Position-clamp experiments*

The instrument was calibrated as described in[54]. In experiments with proportional control in paper **II** latex beads (3 μm, Micromod) were used and in predictive-control experiments in paper **III** polystyrene beads (1.78 μm, Kisker Biotech) were used. Both detection lasers and the steerable trap laser were positioned at the center of the field of view. One detection laser was used 'in-loop' as a feedback signal to the controller, while the other detection laser remained 'out-of-loop'. Only data from the out-of-loop detection channel is shown. The bead and the trap position was then recorded while the controller gains were varied. In proportional control experiments the gain was increased until trapping became unstable at $K_P \gtrsim 25$. In predictive control experiments data was collected with both proportional ($\alpha = 0$) and predictive ($\alpha = 0.013$) control. In experiments with predictive control it was possible to increase the gain beyond $K_P \gtrsim 100$ before trapping became unstable. Measured time series data was analyzed by extracting the position histogram and calculating the position time series PSD. Results were compared with the theoretical PSD predictions for proportional control and predictive control.

2.3.3 *Force-clamp experiments*

Two force clamp experiments were performed in **IV**. In the first experiment a 48 kb double-stranded (ds) DNA construct was held force clamped at 4-40 pN while the feedback gains were varied. In the second experiment the

same construct was force-clamped in the presence of lambda exonuclease, which converts the double-stranded construct into its single-stranded form. Exonucleases are integral parts of many genetic recombination and repair systems. They degrade one strand of double stranded DNA in the 5′ to 3′ direction, leaving non-hydrolyzed single-stranded (ss) DNA and 5′-mononucleotides[27, 55, 56]. When DNA is held at constant force below ~6 pN the ss-form is shorter than the ds-form, and thus the enzymatic activity results in a gradual shortening of the tether.

A 48 kb long DNA construct used in both the experiments was prepared from phage lambda DNA (New England Biolabs) by annealing biotinylated oligonucleotides (Thermo Fischer) at both the 5′- and 3′-ends, essentially as in[57]. Two streptavidin coated polystyrene beads (1.87 µm diameter, Kisker Biotech) were trapped in the first lane of the chamber, transported through the second lane containing DNA at 3.5 pM concentration, where a tether was formed, before entering the third lane for measurement. The first and second lane contained TEW buffer (20 mM Tris pH 8, 1 mM EDTA, 150 mM NaCl, 0.05 mg/ml BSA, and 0.1% Tween20). In force clamp experiments with only DNA the third lane of the chamber contained TEW buffer. In force clamp experiments with lambda exonuclease the third lane contained lambda exonuclease (125 U/ml) in 1x exonuclease reaction buffer (both from New England Biolabs). For the first experiment the flow was stopped during the data collection but in the exonuclease experiments the flow was on (1 µl/min) during the measurement. When a tether was found a force-extension curve was collected in order to distinguish single DNA tethers from multiple tethers. In the first experiment time series of 2 s duration were collected for each gain setting. In the second experiment the tether was force-clamped at 3.4 pN, and data was collected for 20 min, or until the tether broke. In the long duration experiment data was collected at 200 kS/s, then digitally low-pass filtered to 2 kHz on the FPGA, and finally stored to disk at 8 kS/s. The rate of enzymatic activity was calculated by windowing the extension time series into 10 s time intervals with 95% overlap. A first-order polynomial was fit to the data in these windows to obtain velocity estimates.

3

RESULTS

3.1 SNR IN CONSTANT-FORCE EXPERIMENTS

The aim of paper **I** was to investigate under what experimental conditions force clamp experiments (Figure 1) can resolve discrete steps of molecular motors. Figure 6 and 7 summarize results from analysis and simulation of SNR in constant force experiments in **I**.

Figure 6A shows a representative simulated time series, and its low-pass filtered version, from the Brownian dynamics simulation. Steps in the time series are seen as periodic peaks in the pair-wise distance distribution (PWD) (Figure 6B). The SNR can be determined from the normalized peak height in the Fourier transform of the PWD (Figure 6C). Note that due to attenuation of the step length, Eq. (2.4), the peak appears at a spatial frequency exceeding $\omega_{\Delta L} = \frac{2\pi}{\triangle L}$. In order to correctly find the step length from time series data it was found that SNR>4 is required.

Figure 7 shows a contour-plot at SNR=4 extracted from simulations (symbols), the theoretical SNR of Eq. (2.7) (solid lines), and an approximation to the theory (dashed lines, see **I**).

In summary the results of paper **I** show that the analytic exact and approximate SNR expressions agree with the results from the Brownian dynamics simulation. A detection threshold of SNR>4 was found, and the dependence of the SNR on the tether contour length, tether persistence length, motor step rate, motor step length, and clamp force were explored.

3.2 POSITION-CLAMP CONTROL

Real-time position clamping experiments were performed in paper **II** and **III** to investigate how much real-time feedback control can increase the effective trap stiffness. Figure 8 and 9 summarize the results from proportional control position clamp experiments in **II**.

A normalized histogram of the measured position of a position clamped bead is shown in Figure 8. The effective trap stiffness increases from 26 pN/μm at $K_P = 0$ to a maximum of 340 pN/μm at $K_P = 16$, as determined by a gaussian fit to the histogram. The effective trap stiffness thus increases ~13-fold. Note that the histogram shape remains gaussian for all gains, and that the effective trap-stiffness decreases as gain is increased beyond $K_P \gtrsim 16$. The position power spectral density and effective trap stiffness are shown in Figure 9. Solid lines show the theoretically predicted PSD from Eq. (2.14). The PSD has a Lorentzian shape at $K_P = 0$, and as gain is increased the low-frequency components (below ca. 10 kHz) are reduced. At $K_P = 24.8$ a resonance-peak appears at ~10 kHz. This peak grows as

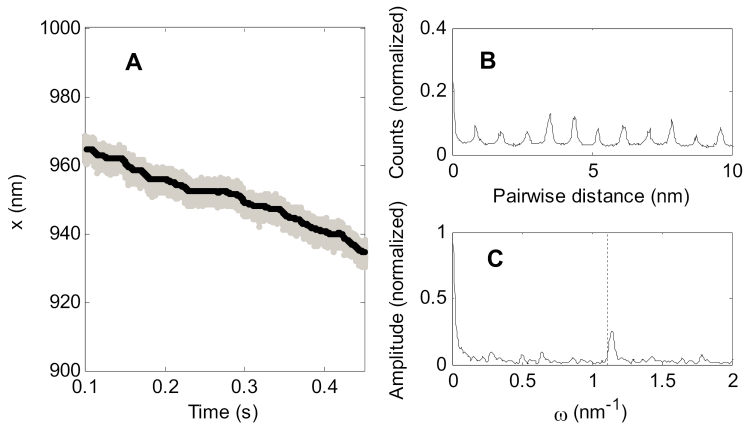

Figure 6: (A) Time-series from Brownian dynamics simulation of experiment in Figure 1. Sampled data in grey, low-pass filtered data in black. (B) PWD of data in (A). (C) Normalized Fourier transform of PWD in (B). The dashed vertical line in (C) indicates the spatial frequency $\omega_{\Delta L} = \frac{2\pi}{\triangle L}$.

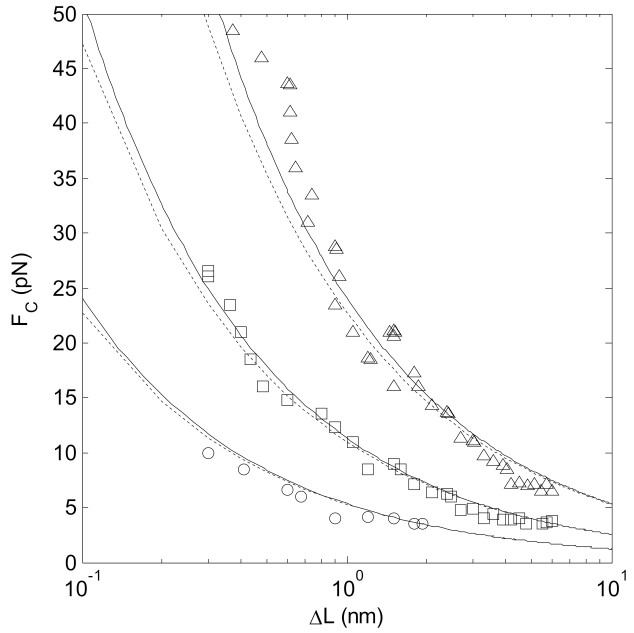

Figure 7: Contour-plot of SNR=4, the step length detection limit, in constant-force experiment (Figure 1) with varying step length $\triangle L$ and clamp-force F_C. Three different enzymatic rates are shown, $k_{cat} = 10\,\mathrm{s}^{-1}$ (circles), $k_{cat} = 100\,\mathrm{s}^{-1}$ (squares), and $k_{cat} = 1000\,\mathrm{s}^{-1}$ (triangles). The solid lines indicate SNR=4 as predicted by Eq. (2.7). The dashed lines indicate SNR=4 as predicted by the approximations presented in **I**. Symbols indicate SNR=4 determined with Eq. (2.11) from simulated time-series. Simulation parameters: WLC contour-length $L = 1000\,\mathrm{nm}$, persistence length $L_P = 50\,\mathrm{nm}$, and bead diameter $d = 1000\,\mathrm{nm}$.

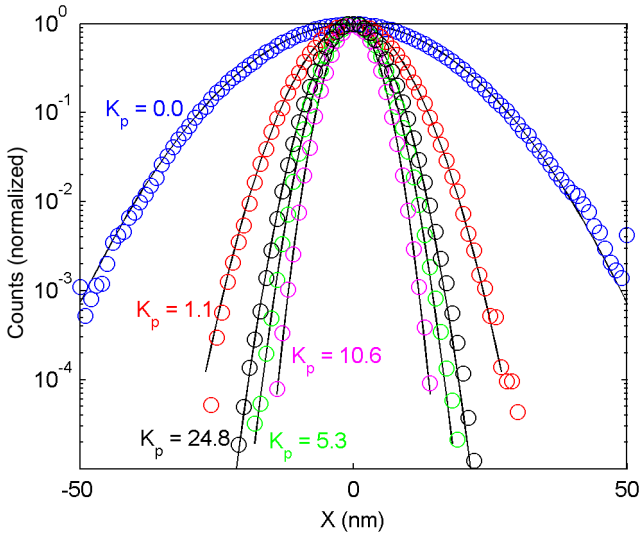

Figure 8: Measured position histogram for position clamped bead using proportional control with gain K_P. Gaussian fits to data (solid lines) indicate harmonic trapping.

gain is further increased and eventually leads to unstable trapping and loss of the bead. The inset in Figure 9 shows the effective trap stiffness as a function of gain.

Figure 10 and 11 summarize results from experiments with predictive-control in **III**.

While the PSD with proportional control (Figure 10A) shows a resonance peak which limits the maximum attainable gain, the PSD with predictive control (Figure 10B) does not show a resonance peak, and gain can therefore be increased to $K_P > 100$ while retaining stable trapping. The theoretical predictions for the PSDs (Eq. (2.14) and Eq. (2.16)) agree with experimental data except for a $1/f$ tail seen in the experimental data at low frequencies and high gains. For the same trapping laser power and bead, predictive control increased the effective trap-stiffness 9.6-fold at $K_P \approx 80$, while the effective stiffness increased 6.2-fold at best using $K_P \approx 13$ with proportional control (Figure 11).

In summary the results from **II** and **III** show that AOD-based trap steering with FPGA-based real-time control can increase the effective trap stiffness by roughly 10-fold.

3.3 FORCE-CLAMP CONTROL

Paper **IV** uses real-time control to maintain a constant tether-tension in a dumbbell experiment (Figure 2, bottom). We ask how tether tension and extension fluctuate during force clamping, and if the instrument can be used for constant force experiments in single molecule biology. Figure 12 and 13 summarize the results of force-clamp experiments in **IV**.

The PSD of force fluctuations in the stationary trap (Figure 2) using different proportional- and integral- gains is shown in Figure 12. A reduction

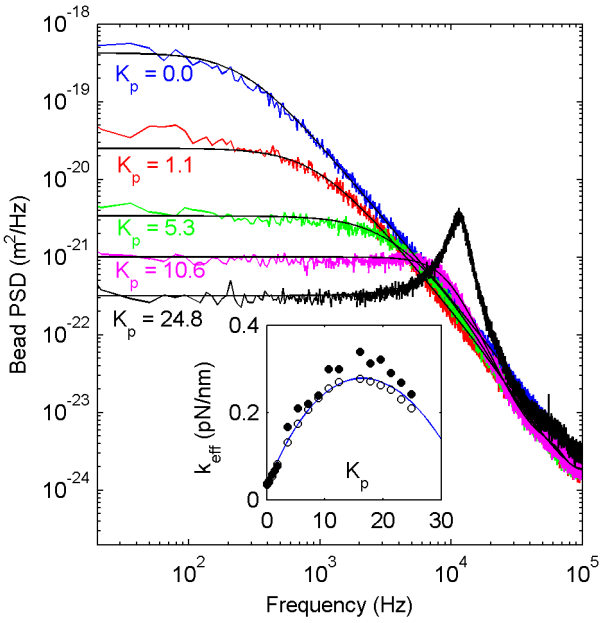

Figure 9: Measured PSD of position fluctuations for position clamped bead with proportional control. The predicted PSD for each gain setting, Eq. (2.14), is shown as a solid line. The inset shows the effective trap stiffness as a function of gain as determined from the Gaussian fits in Figure 8 (open symbols), and alternatively calculated by integrating the PSD (closed symbols). The theoretical prediction (Eq. (2.14) inserted into Eq. (2.17)) is shown as a solid line.

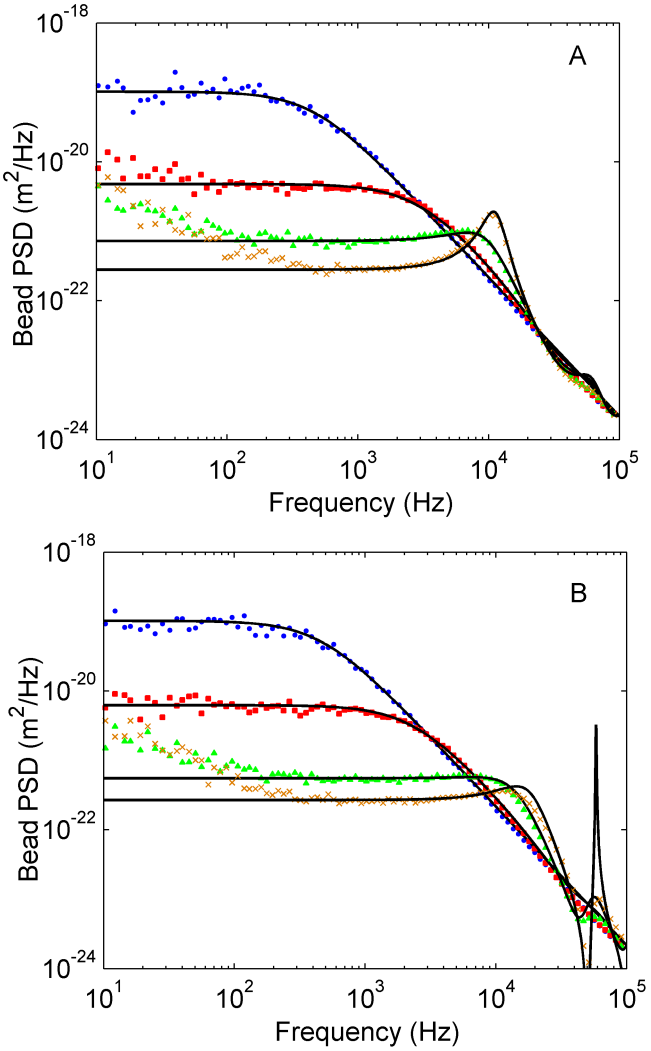

Figure 10: Measured bead position PSD for position-clamp with (A) proportional-, and (B) predictive- control. Solid lines show theoretically predicted PSDs from Eq. (2.14) and Eq. (2.16). Data is shown for (from top to bottom) $K_P = 0$, $K_P = 3.6$, $K_P = 10.9$, $K_P = 18.1$ in A, and for $K_P = 0$, $K_P = 3.6$, $K_P = 27.2$, $K_P = 79.8$ in B.

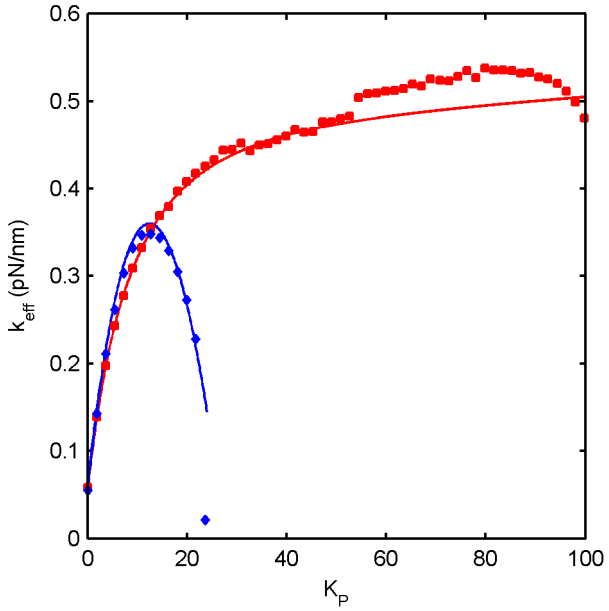

Figure 11: Effective trap stiffness for position-clamp with proportional control (blue), and predictive control (red). Symbols show measured effective trap stiffness. Lines indicate theoretical predictions calculated by inserting Eq. (2.14) and Eq. (2.16) into Eq. (2.17).

in the force noise is seen especially at low frequencies, where the PSD is proportional to f^2, as predicted by Eq. (2.24).

The results of a force clamp experiment in the presence of lambda exonuclease is shown in Figure 13. The DNA-construct was force clamped at 3.4 pN using $K_P = 0$ and $K_I = 0.0004$, while the change in extension was monitored during ~800 s. Figure 13A and B show measured time-series of the tether tension and extension, respectively. The tether tension remained within 3.4 ± 0.4 pN during the experiment, while the extension decreased from $\sim 15.5\,\mu$m to $8\,\mu$m. Figure 13C and D show the rate of change in the extension and the rate histogram, respectively. The average tether extension shortening rate during the experiment was 9 ± 6 nm/s. Assuming a 14 μm length change during 48 kb of translocation[57] this corresponds to a translocation velocity of 30 ± 20 nt/s for the enzyme along the DNA. No discrete steps were observed in the time series data, and assuming that lambda exonuclease moves along DNA in discrete steps of 0.34 nm length (one base-pair), a rough estimate of the SNR in this experiment using Eq. (25) in **I** shows that SNR<<1. Negative control experiments with the same DNA construct force-clamped under the same experimental conditions but in the absence of lambda exonuclease showed no extension change.

In summary the results from **IV** show that the experimental real-time force clamp dynamics agree with predictions (Eq. (2.24)) and that the instrument has successfully been used for constant-force experiments in single molecule biology.

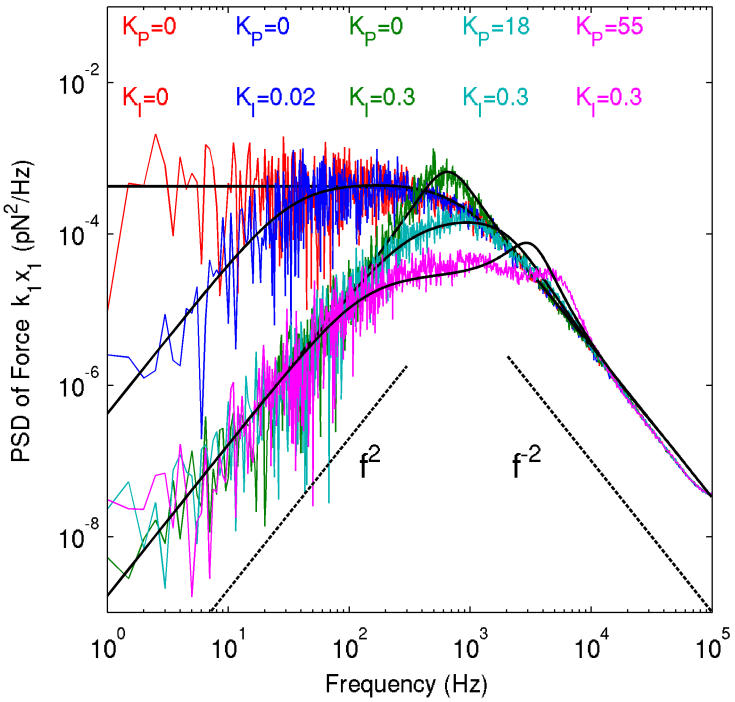

Figure 12: Power spectral density of force fluctuation during a force clamp experiment (6 pN set-point force). Solid lines indicate the theoretical prediction, from Eq. (2.24). Dashed lines proportional to f^2 and f^{-2} serve as a guide to the eye.

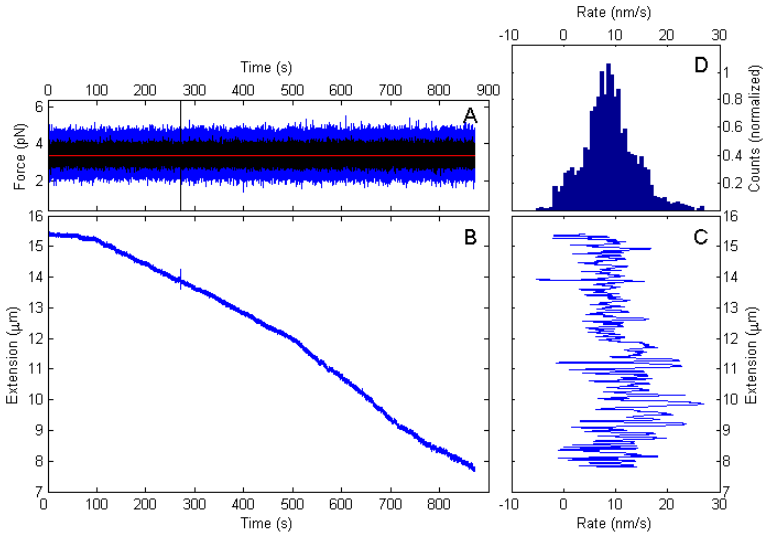

Figure 13: (A) tether tension and (B) extension of force clamped DNA construct in presence of lambda exonuclease. In (A) the blue trace shows data collected at 2 kHz. The black trace shows the same data low-pass filtered to 100 Hz. The force set-point, 3.4 pN, is shown in red. (C) rate of extension change calculated from the time series in (A). (D) histogram of extension rate with average $9 \pm 6\,\mathrm{nm/s}$.

4

DISCUSSION

4.1 SNR IN CONSTANT-FORCE EXPERIMENTS CAN BE PREDICTED

Measurements that hope to reveal discrete steps in molecular mechanisms with experiments similar to that in Figure 1 must overcome two obstacles. First, the bead position signal is attenuated due to the finite tether stiffness (Eq. (2.4)). Only a fraction corresponding to the relative tether extension (x_e/L) of the true step length is observed. Second, the signal is obscured by thermal noise which complicates experiments when the step length is comparable to bead fluctuations caused by thermal noise (Eq. (2.6)). In practice often either the effective stiffness k_{DNA} is increased by use of a higher clamp-force, or the measurement bandwidth f_{LP} is reduced in order to low-pass filter the zero-mean thermal noise. A threshold signal-to-noise ratio of SNR>4, at which the step length could be correctly extracted from simulated time-series, was found in **I**. To summarize, maximum SNR in step length experiments is achieved with small beads using short stiff tethers at high tension in a cold environment. A slow molecular motor with a long step length is preferable. A comparison of the predicted SNR (Eq. (2.7)) and the approximations in **I** with experimental data (**I,** Table 2) indicates that the developed expressions can reliably be used to estimate SNR in experiments.

The main contribution of paper **I** is to extend the results of [33] by providing SNR formulas, validated by simulations as well as by comparisons with experiments, which take into account the force dependent stiffness of a WLC tether. The developed theory/simulation does not account for instrument drift, usually $1/f$ (pink) noise, which in practice degrades SNR.

4.2 POSITION-CLAMP CONTROL CAN INCREASE EFFECTIVE TRAP STIFFNESS

The position clamp results in **II** and **III** indicate that the effective trap stiffness can be increased by one order of magnitude using proportional or predictive control. Predictive control delays the onset of unstable trapping associated with the resonance peak in the PSD - allowing higher gains to be used which leads to higher effective stiffness. For both control schemes the loop-delay, i.e. the time it takes to measure the bead position and act on this information by steering the trap, limits the maximum effective stiffness that can be achieved. In our instrument the total delay of ~19 μs consists mainly of the acoustic time of flight in the AOD, ca 10 μs, and the analog to digital conversion time, 5 μs, of the data acquisition card. The predicted PSDs, Eq. (2.14) and Eq. (2.16), agree with experimental data, and can thus

with some confidence be used to predict the dynamics future position clamp experiments with our instrument or similar experiments with other instruments.

The main contribution of paper **II** is to show that effective trap stiffness can be increased 10-fold using position clamp control, and that the bead position PSD can be predicted. Paper **III** extends these results by presenting a predictive control algorithm.

4.3 FORCE CLAMP CONTROL ALLOWS CONSTANT FORCE SINGLE MOLECULE EXPERIMENTS

The presented active real-time optical force clamp in **IV** maintains a constant 0-100 pN tension in a dumbbell-tether while allowing for tether extension changes of several micrometers. The predicted position and force PSDs, Eq. (2.24), agree with experimental data. It is thus possible to predict what effect varying the instrument bandwidth, the loop delay, the set-point force, and the feedback gains will have on the shape of the PSD. This allows designing real-time force clamp experiments that balance the trade-off between the conflicting requirements of constant tether tension and low uncertainty in the tether extension. The results from the experiment with lambda exonuclease shows that the instrument can track extension changes over several micrometers at constant tension. The observed translocation velocity of 30 ± 20 nt/s agrees with previous bulk[56] and single molecule[27] experiments. Consistent with SNR<<1, no steps were observed in the data. The broad velocity-distribution (Figure 13D) is an indication of dynamic heterogeneity. Pausing [27] was also observed (data not shown), but not analyzed further.

The main contribution of paper **IV** is to demonstrate an experimental real-time force clamp and a model that describes the dynamics of the experiment. Observing the enzymatic activity of lambda exonuclease serves as a proof-of-principle constant force experiment in single molecule biology.

4.4 CONCLUSIONS

The main goal, to construct, calibrate, test, and perform a proof-of-principle experiment in single molecule biology with a double-trap optical tweezers instrument was achieved. The developed instrument can be used to investigate the molecular mechanics of a wide variety of molecular motors and protein/nucleic-acid interactions.

The results of the study indicate that the presented models for SNR in constant-force experiments and for beads in feedback-controlled optical tweezers agree with experiments. The effective trap stiffness can be increased by an order of magnitude using the presented position-clamping method. The force-clamp can be used for constant force experiments, and a successful proof-of-principle experiment with lambda exonuclease was

performed. The developed instrument serves as a stepping stone for future contributions to the growing field of single molecule biology.

REFERENCES

[1] J. Howard. *Mechanics of Motor Proteins and the Cytoskeleton*. Sinauer Associates, 2001. ISBN 0-87893-334. (Cited on page 1.)

[2] K. C. Neuman and A. Nagy. Single-molecule force spectroscopy: optical tweezers, magnetic tweezers and atomic force microscopy. *Nature methods*, 5 (6):491–505, 2008. doi:10.1038/nmeth.1218. (Cited on page 1.)

[3] A. Ashkin. Acceleration and trapping of particles by radiation pressure. *Physical Review Letters*, 24:156–159, 1970. doi:10.1103/PhysRevLett.24.156. (Cited on page 1.)

[4] A. Ashkin and J. M. Dziedzic. Feedback stabilization of optically levitated particles. *Appl. Phys. Lett.*, 30(4):202–204, 1977. doi:10.1063/1.89335. (Cited on pages 1 and 2.)

[5] A. Ashkin, J. M. Dziedzic, J. E. Bjorkholm, and S. Chu. Observation of a single-beam gradient force optical trap for dielectric particles. *Optics Letters*, 11(5):288–290, 1986. doi:10.1364/OL.11.000288. (Cited on page 1.)

[6] A. Alessandrini and P. Facci. Afm: a versatile tool in biophysics. *Measurement Science and Technology*, 16(6):R65, 2005. doi:10.1088/0957-0233/16/6/R01. (Cited on page 1.)

[7] T. R. Strick, J.-F. Allemand, D. Bensimon, A. Bensimon, and V. Croquette. The elasticity of a single supercoiled dna molecule. *Science*, 271:1835–1837, 1996. doi:10.1126/science.271.5257.1835. (Cited on page 1.)

[8] A. Crut, D. A. Koster, R. Seidel, C. H. Wiggins, and N. H. Dekker. Fast dynamics of supercoiled dna revealed by single-molecule experiments. *Proceedings of the National Academy of Sciences*, 104(29):11957–11962, 2007. doi:10.1073/pnas.0700333104. (Cited on page 1.)

[9] M. J. Lang and S. M. Block. Resource letter: Lbot-1: Laser-based optical tweezers. *American Journal of Physics*, 71:201–215, 2003. doi:10.1119/1.1532323. (Cited on page 1.)

[10] K. C. Neuman and S. M. Block. Optical trapping. *Review of Scientific Instruments*, 75(9):2787–2809, 2004. doi:10.1063/1.1785844. (Cited on page 1.)

[11] T. T. Perkins. Optical traps for single molecule biophysics: a primer. *Laser & Photon. Rev.*, 3(1-2):203–220, 2008. doi:10.1002/lpor.200810014. (Cited on page 1.)

[12] J. Zlatanova and K. van Holde. Single-molecule biology: What is it and how does it work? *Molecular Cell*, 24:317–329, 2006. doi:10.1016/j.molcel.2006.10.017. (Cited on page 1.)

[13] A. N. Kapanidis and T. Strick. Biology, one molecule at a time. *Trends in Biochemical Sciences*, 34(5):234 – 243, 2009. doi:10.1016/j.tibs.2009.01.008. (Cited on page 1.)

[14] W. J. Greenleaf, M. T. Woodside, and S. M. Block. High-resolution, single-molecule measurements of biomolecular motion. *Annu. Rev. Biophys. Biomol. Struct.*, 36:171–190, 2007. doi:10.1146/annurev.biophys.36.101106.101451. (Cited on page 1.)

[15] N. G. Walter, C.-Y. Huang, A. J. Manzo, and M. A. Sobhy. Do-it-yourself guide: how to use the modern single-molecule toolkit. *Nat Meth*, 5(6):475–489, 2008. doi:10.1038/nmeth.1215. (Cited on page 1.)

[16] A. M. van Oijen. Cutting down the forest to see a single tree. *Nature Chemical Biology*, 4:440–443, 2008. doi:10.1038/nchembio0808-440. (Cited on page 1.)

[17] A. E. Knight. *Single Molecule Biology*. Academic Press, 2009. ISBN 978-0-12-374227-8. (Cited on page 1.)

[18] K. Svoboda and S. M. Block. Biological applications of optical forces. *Annual Review of Biophysics and Biomolecular Structure*, 23(1):247–285, 1994. doi:10.1146/annurev.bb.23.060194.001335. (Cited on page 1.)

[19] A. Ashkin. Forces of a single-beam gradient laser trap on a dielectric sphere in the ray optics regime. *Biophysical journal*, 61:569–582, 1992. doi:10.1016/S0006-3495(92)81860-X. (Cited on page 1.)

[20] A. Rohrbach. Stiffness of optical traps: Quantitative agreement between experiment and electromagnetic theory. *Phys. Rev. Lett.*, 95(16):168102, 2005. doi:10.1103/PhysRevLett.95.168102. (Cited on page 1.)

[21] M. J. Lang, C. L. Asbury, J. W. Shaevitz, and S. M. Block. An automated two-dimensional optical force clamp for single molecule studies. *Biophys. J.*, 83:491–501, 2002. doi:10.1016/S0006-3495(02)75185-0. (Cited on pages 1 and 2.)

[22] G. J. Wuite, R. J. Davenport, A. Rappaport, and C. Bustamante. An integrated laser trap/flow control video microscope for the study of single biomolecules. *Biophys J*, 79(2):1155–67, 2000. doi:10.1016/S0006-3495(00)76369-7. (Cited on pages 1 and 2.)

[23] K. C. Neuman, E. H. Chadd, G. F. Liou, K. Bergman, and S. M. Block. Characterization of photodamage to escherichia coli in optical traps. *Biophys. J.*, 77: 2856–2863, 1999. doi:10.1016/S0006-3495(99)77117-1. (Cited on page 1.)

[24] W. Grange, S. Husale, H.-J. Guntherodt, and M. Hegner. Optical tweezers system measuring the change in light momentum flux. *Review of Scientific Instruments*, 73(6):2308–2316, 2002. doi:10.1063/1.1477608. (Cited on page 1.)

[25] F. Gittes and C. F. Schmidt. Interference model for back-focal-plane displacement detection in optical tweezers. *Optics Letters*, 23(1):7–9, 1998. doi:10.1364/OL.23.000007. (Cited on page 2.)

[26] A. R. Carter, G. M. King, and T. T. Perkins. Back-scattered detection provides atomic-scale localization precision, stability, and registration in 3d. *Optics Express*, 15:13434–13445, 2007. doi:10.1364/OE.15.013434. (Cited on page 2.)

[27] T. T. Perkins, R. V. Dalal, P. G. Mitsis, and S. M. Block. Sequence-dependent pausing of single lambda exonuclease molecules. *Science*, 301(5641):1914–8, 2003. doi:10.1126/science.1088047. (Cited on pages 2, 15, and 26.)

[28] D. E. Smith, S. J. Tans, S. B. Smith, S. Grimes, D. L. Anderson, and C. Bustamante. The bacteriophage fi29 portal motor can package dna against a large internal force. *Nature*, 413:748–752, 2001. doi:10.1038/35099581. (Cited on page 2.)

[29] M. Klein, M. Andersson, O. Axner, and E. Fallman. Dual-trap technique for reduction of low-frequency noise in force measuring optical tweezers. *Appl. Opt.*, 46:405–412, 2007. doi:10.1364/AO.46.000405. (Cited on page 2.)

[30] D. G. Grier. A revolution in optical manipulation. *Nature Photonics*, 424: 810–816, 2003. doi:10.1038/nature01935. (Cited on page 2.)

[31] E. A. Abbondanzieri, W. J. Greenleaf, J. W. Shaevitz, R. Landick, and S. M. Block. Direct observation of base-pair stepping by rna polymerase. *Nature*, 438(24):460–465, 2005. doi:10.1038/nature04268. (Cited on page 2.)

[32] R. T. Dame, M. C. Noom, and G. J. L. Wuite. Bacterial chromatin organization by h-ns protein unraveled using a dual dna assay. *Nature*, 444:387–390, 2006.

doi:10.1038/nature05283. (Cited on page 2.)

[33] F. Gittes and C. F. Schmidt. Thermal noise limitations on micromechanical experiments. *Eur. Biophys. J.*, 27:75–81, 1998. doi:10.1007/s002490050113. (Cited on pages 2 and 25.)

[34] J. Bechhoefer. Feedback for physicists: A tutorial essay on control. *Rev. Mod. Phys.*, 77(3):783–836, 2005. doi:10.1103/RevModPhys.77.783. (Cited on page 2.)

[35] K. Visscher and S. Block. Versatile optical traps with feedback control. *Methods In Enzymology*, 298:460–489, 1998. doi:10.1016/S0076-6879(98)98040-5. (Cited on page 2.)

[36] K. Visscher, M. J. Schnitzer, and S. M. Block. Single kinesin molecules studied with a molecular force clamp. *Nature*, 400:184–189, 1999. doi:10.1038/22146. (Cited on page 2.)

[37] M. D. Wang, H. Yin, R. Landick, J. Gelles, and S. M. Block. Stretching dna with optical tweezers. *Biophysical Journal*, 72(3):1335–46, 1997. doi:10.1016/S0006-3495(97)78780-0. (Cited on page 2.)

[38] R. M. Simmons, J. T. Finer, S. Chu, and J. A. Spudich. Quantitative measurements of force and displacement using an optical trap. *Biophysical Journal*, 70: 1813–1822, 1996. doi:10.1016/S0006-3495(96)79746-1. (Cited on page 2.)

[39] K. D. Wulff, D. G. Cole, and R. L. Clark. Adaptive disturbance rejection in an optical trap. *Appl. Opt.*, 47(20):3585–3589, 2008. doi:10.1364/AO.47.003585. (Cited on page 2.)

[40] D. Preece, R. Bowman, A. Linnenberger, G. Gibson, S. Serati, and M. Padgett. Increasing trap stiffness with position clamping in holographic optical tweezers. *Opt. Express*, 17(25):22718–22725, 2009. doi:10.1364/OE.17.022718. (Cited on page 2.)

[41] Y. Huang, J. Wan, M.-C. Cheng, Z. Zhang, S. M. Jhiang, and C.-H. Menq. Three-axis rapid steering of optically propelled micro/nanoparticles. *Review of Scientific Instruments*, 80(6):063107, 2009. doi:10.1063/1.3156838. (Cited on page 2.)

[42] Y. Huang, Z. Zhang, and C.-H. Menq. Minimum-variance brownian motion control of an optically trapped probe. *Appl. Opt.*, 48(30):5871–5880, 2009. doi:10.1364/AO.48.005871. (Cited on page 2.)

[43] R. Nambiar, A. Gajraj, and J.-C. Meiners. All-optical constant-force laser tweezers. *Biophysical Journal*, 87:1972–1980, 2004. doi:10.1529/biophysj.103.037697. (Cited on page 2.)

[44] W. J. Greenleaf, M. T. Woodside, E. A. Abbondanzieri, and S. M. Block. Passive all-optical force clamp for high-resolution laser trapping. *Physical Review Letters*, 95:208102, 2005. doi:10.1103/PhysRevLett.95.208102. (Cited on page 2.)

[45] Y.-F. Chen, G. A. Blab, and J.-C. Meiners. Stretching submicron biomolecules with constant-force axial optical tweezers. *Biophysical Journal*, 96:4701–4708, 2009. doi:10.1016/j.bpj.2009.03.009. (Cited on page 2.)

[46] M. T. Woodside, P. C. Anthony, W. M. Behnke-Parks, K. Larizadeh, D. Herschlag, and S. M. Block. Direct measurement of the full sequence-dependent folding landscape of a nucleic acid. *Science*, 314:1001, 2006. doi:10.1126/science.1133601. (Cited on page 2.)

[47] H. Press. *Numerical Recipes in C*. Cambridge University Press, Cambridge, 1988. (Cited on page 7.)

[48] M. Matsumoto and T. Nishimura. Mersenne twister: a 623-dimensionally equidistributed uniform pseudo-random number generator. *ACM Transactions*

on Modeling and Computer Simulation, 8:3–30, 1998. doi:10.1145/272991.272995. (Cited on page 7.)

[49] E.-P. Box, G. and E. Muller, M. A note on the generation of random normal deviates. *The Annals of Mathematical Statistics*, 29:610–611, 1958. doi:10.1214/aoms/1177706645. (Cited on page 7.)

[50] K. Berg-Sorensen and H. Flyvbjerg. Power spectrum analysis for optical tweezers. *Review of Scientific Instruments*, 75(3):594–612, 2004. doi:10.1063/1.1645654. (Cited on page 7.)

[51] J. R. Moffitt, Y. R. Chemla, D. Izhaky, and C. Bustamante. Differential detection of dual traps improves the spatial resolution of optical tweezers. *Proc. Natl. Acad. Sci. USA.*, 103:9006–9011, 2006. doi:10.1073/pnas.0603342103. (Cited on page 9.)

[52] D. L. Ermak and J. A. McCammon. Brownian dynamics with hydrodynamic interactions. *The Journal of Chemical Physics*, 69(4):1352–1360, 1978. doi:10.1063/1.436761. (Cited on page 9.)

[53] H. Ojala. Stiffer optical tweezers through real-time feedback control. Master's thesis, University of Helsinki, 2007. URL `http://urn.fi/URN:NBN:fi-fe20072155`. (Cited on page 13.)

[54] A. E. Wallin, H. Ojala, A. Korsback, E. Haeggstrom, and R. Tuma. Real-time control of optical tweezers. *Proc. SPIE*, 6644:66441Y, 2007. doi:10.1117/12.737269. (Cited on page 14.)

[55] P. G. Mitsis and J. G. Kwagh. Characterization of the interaction of lambda exonuclease with the ends of dna. *Nucleic acids research*, 27(15):3057–3063, 1999. doi:10.1093/nar/27.15.3057. (Cited on page 15.)

[56] K. Subramanian, W. Rutvisuttinunt, W. Scott, and R. S. Myers. The enzymatic basis of processivity in lambda exonuclease. *Nucleic acids research*, 31(6):1585–1596, 2003. doi:10.1093/nar/gkg266. (Cited on pages 15 and 26.)

[57] N. A. Tanner and A. M. V. Oijen. Single-molecule observation of prokaryotic dna replication. *Methods in Molecular Biology*, 521:397–410, 2009. doi:10.1007/978-1-60327-815-7_22. (Cited on pages 15 and 22.)

A

APPENDIX: BROWNIAN DYNAMICS SIMULATION

This appendix contains pseudo-code for the Brownian dynamics simulation presented in 2.1.2. The C source code is available from the author by email. The simulation requires three external functions: **genrandn()** returns a normally distributed pseudo random number with zero mean and unit variance. **dwellTimeDistribution()** returns an exponentially distributed pseudo random number corresponding to the enzymatic rate k_{cat}. **WLC(L,x,y,z)** returns the xyz-components of force on the bead due to the worm-like chain, given the current contour length L and the position of the bead.

Algorithm 1 Brownian dynamics simulation.

$n \leftarrow 0$ {the current simulation step}
$Nsim \leftarrow t_{max} / \triangle t$ {set max number of simulation steps}
$time \leftarrow 0$
$step \leftarrow 0$ {the number of steps taken by the molecular motor}
$endstepValid \leftarrow$ **false**
$L \leftarrow L_0$ {initialize length of WLC}
$(x, y, z) \leftarrow (0, 0, 0)$ {initialize the bead position}
while $n \leq Nsim$ **do**
  (I. store current values of x,y,z,L to disk for later analysis)
  (II. generate random displacement of bead)
  $r \leftarrow \sqrt{2 \triangle t k_B T / \gamma}$
  $(r_x, r_y, r_z) \leftarrow (r \cdot \mathbf{genrandn}(), r \cdot \mathbf{genrandn}(), r \cdot \mathbf{genrandn}()$
  (III. compute time for next motor-step, if necessary)
  if *endstepValid* is **false then**
    $\tau \leftarrow \mathbf{dwellTimeDistribution}()$
    $endstep \leftarrow time + \tau$ {the next step occurs at this time}
    $endstepValid \leftarrow$ **true**
  end if
  (IV. take a motor-step, if it is time)
  if $time > endstep$ **then**
    $step \leftarrow step + 1$
    $L \leftarrow L_0 - step \cdot \triangle L$
    $endstepValid \leftarrow$ **false**
  end if
  (V. calculate forces on bead)
  $(F_{WLC,x}, F_{WLC,y}, F_{WLC,z}) \leftarrow \mathbf{WLC}(\mathbf{L}, \mathbf{x}, \mathbf{y}, \mathbf{z})$
  $(F_{OT,x}, F_{OT,y}, F_{OT,z}) \leftarrow (F_C, -k \cdot y, -k \cdot z)$
  (VI. update bead position)
  $x \leftarrow x + \frac{\triangle t}{k_B T \gamma} \cdot (F_{OT,x} + F_{WLC,x}) + r_x$
  $y \leftarrow y + \frac{\triangle t}{k_B T \gamma} \cdot (F_{OT,y} + F_{WLC,y}) + r_y$
  $z \leftarrow z + \frac{\triangle t}{k_B T \gamma} \cdot (F_{OT,z} + F_{WLC,z}) + r_z$
  $n \leftarrow n + 1$
  $time \leftarrow time + \triangle t$
end while

B

APPENDIX: OPTICAL TWEEZERS COMPONENTS

Component	Manufacturer	Model
1064 (trap laser)	Coherent	Compass 1064-4000
SH1, SH2 (shutters)	Thorlabs	SH05
FI1 (Faraday isolator for trap laser)	Linos, FI	FI-1064
FI2, FI3 (Faraday isolators for detection lasers)	Linos	DLI-1
PBS1, PBS2 (polarizing beam splitters)	Newport	05BC16PC.9
PBS3 (polarizing beam splitter)	Newport	05FC16PB.5
PBS4 (polarizing beam splitter)	Newport	10FC16PB.5
785 (detection laser, 785 nm)	Hitachi	HL7851G
830 (detection laser, 830 nm)	Thorlabs	DL5032-001
D1 (dichroic mirror)	CVI	SWP-45-RU1064-TU850-PW-2025-C
D2 (dichroic mirror)	Chroma	780DCSPXR
D3 (dichroic mirror)	CVI	TLM2-800-45-UNP-2037
SMF (single-mode polarization-maintaining optical fiber)	Nufern	PM780-HP
OC (output coupler)	Thorlabs	F810APC-780
HWP2, HWP3 (half-wave plates)	Thorlabs	WPMH05M-780
HWP4, HWP5 (half-wave plates)	Thorlabs	WPMH05M-830
OBJ (microscope objective)	Nikon	100x TIRF oil, N.A. 1.49
COND (microscope condensor)	Nikon	HNA-OIL, N.A. 1.4
F1 (cold mirror)	Thorlabs	FM203
F2 (laser-line filter, 830nm)	Semrock	LL01-830
F3 (laser-line filter, 785nm)	Thorlabs	FL780-10
F4, F5 (filters)	Schott	KG1 and KG3
L1:L2, 1:1 telescope (lens)	Thorlabs	f=50 mm
L3:L4 (lens)	Thorlabs	f=500 mm
L5:L6 (lens)	Thorlabs	f=100 mm
L7:L8 (lens)	Thorlabs	f=500 mm

Table 1: Components of optical tweezers instrument. See Figure 3 and 4.

Component	Manufacturer	Model
PD1, PD2 (position sensitive photodiodes)	SiTek	S2-0171
AOD (acousto-optic deflector)	NEOS-Technologies	45035-3-6.5DEG-1.06-XY
DDS (digital direct synthesizer RF generator)	NEOS-Technologies	64010-200-2AMDFS
PZT1 (piezo-motor XY microscope stage)	Physik Instrumente	M-686.D64 with C-867.D64 controller
PZT2 (piezo-electric XYZ microscope stage)	Physik Instrumente	P-517.3CD with E-710.3CD controller
FPGA (data-acquisition card with field-programmable gate array)	National Instruments	PCI-7833R
AMP (variable-gain instrumentation amplifier)	Burr-Brown	INA111
CCD (camera)	Panasonic	WV-BP100/G

Table 2: Electronics of optical tweezers instrument. See Figure 3 and 4.

C

APPENDIX: PREDICTIVE CONTROL

This appendix motivates the formula for the position estimate x_p for $x(t+\tau)$ in Eq. (2.15), used for predictive position-clamp control. An ideal proportional position clamp with $x_{set} = 0$ would steer the trap according to

$$x_T(t+\tau) = -K_P x(t+\tau), \tag{C.1}$$

where τ is the loop delay time. However, since $x(t+\tau)$ is unknown when the control algorithm runs, any real controller must act only on past measurements of x in agreement with Eq. (2.13). The predicted position x_p is derived assuming that the trap is steered by a digital controller with sampling interval $\triangle$. On the hardware used for this study $\tau = 3\Delta$, which is assumed throughout the discussion here. An estimate for $x(t+\Delta)$ can be obtained by assuming that the time-average of thermal forces during the sampling interval vanishes. The equation of motion then simplifies to

$$\gamma\dot{x} - k(x - x_T) = 0\,, \tag{C.2}$$

with the solution

$$x(t+\Delta) = x(t) + \alpha\left[x(t) - x_T(t)\right]\,, \tag{C.3}$$

where $\alpha = 1 - \exp\left(-k\triangle/\gamma\right)$. To obtain $x(t+\tau) = x(t+3\triangle)$ we can substitute iteratively from Eq. (C.3) three times:

$$\begin{aligned}
&x(t+3\triangle) = x(t+2\triangle) - \alpha\left[x(t+2\triangle) - x_T(t+2\triangle)\right] \\
&= x(t+\triangle) - \alpha\left[x(t+\triangle) - x_T(t+\triangle)\right] \\
&- \alpha\left\{x(t+\triangle) - \alpha\left[x(t+\triangle) - x_T(t+\triangle)\right] - x_T(t+2\triangle)\right\} \\
&= x(t) - \alpha\left[x(t) - x_T(t)\right] - \alpha\left[x(t) - \alpha\left[x(t) - x_T(t)\right] - x_T(t+\triangle)\right] \\
&- \alpha\left\{x(t) - \alpha\left[x(t) - x_T(t)\right] - x_T(t+2\triangle) - \right. \\
&\left. -\alpha\left[x(t) - \alpha\left[x(t) - x_T(t)\right] - x_T(t+\triangle)\right]\right\} \\
&\qquad \approx x(t) - \alpha\left[3x(t) - x_T(t) - x_T(t+\triangle) - x_T(t+2\triangle)\right]\,,
\end{aligned} \tag{C.4}$$

where in the last step only terms linear in α have been retained. A change of variable $t' = t + 3\triangle$ now yields Eq. (2.15).